Journal of Saudi Chemical Society (2020) **24**, 896–905

King Saud University

Journal of Saudi Chemical Society

www.ksu.edu.sa
www.sciencedirect.com

ORIGINAL ARTICLE

Functionalization effect of Fe-type MOF for methylene blue adsorption

Syafikah Huda Paiman [a], Mukhlis A. Rahman [a,*], Tetsuo Uchikoshi [b], Norfadhilatuadha Abdullah [a], Mohd Hafiz Dzarfan Othman [a], Juhana Jaafar [a], Khairul Hamimah Abas [c], Ahmad Fauzi Ismail [a]

[a] *Advanced Membrane Technology Research Centre (AMTEC), Universiti Teknologi Malaysia, 81310 Skudai, Johor, Malaysia*
[b] *Material Processing Unit, Fine Particles Engineering Group, National Institute for Materials Science (NIMS), 1-2-1 Sengen, Tsukuba, Ibaraki 305-0047 Japan*
[c] *Faculty of Engineering, Universiti Teknologi Malaysia, 81310 Skudai, Johor, Malaysia*

Received 23 July 2020; revised 11 September 2020; accepted 21 September 2020
Available online 1 October 2020

KEYWORDS

Metal–organic frameworks;
MOF-Fe;
Amine-MOF-Fe;
Adsorption;
Methylene blue

Abstract Water pollutant such as dyes had danger the water quality. Todays, porous materials are great potential for dye adsorption from water bodies. In this study, the iron-based metal–organic framework (MOF-Fe) of MIL-101 is synthesized through a facile solvothermal method. The amine-functionalization effect of the MOF-Fe (amine-MOF-Fe) is evaluated for the adsorptive removal of methylene blue (MB) from aqueous solution. The adsorption behaviour had shown a rapid MB adsorption within the first hour of the process due to the pore-filling mechanism of the porous MOF-Fe structure. The electrostatic interaction between the amino group of amine-MOF-Fe and MB had contributed to the high adsorption capacity. The amine-functionalization effect also found the amine-MOF-Fe is having two times higher adsorption capacity when used with the loading two times lower than non-functionalized MOF-Fe. The maximum equilibrium adsorption capacities were measured at 149.25 and 312.5 mg/g with optimum MOFs loading of 0.8 and 0.4 g/L for MOF-Fe and amine-MOF-Fe, respectively. The adsorption mechanism proposed includes the electrostatic interaction, pore filling, hydrogen bonding, and π–π stacking. The regeneration study showed the MOFs could be recycled without interfering with the removal efficiency. Hence, the results indicate that the MOFs had desirable reusability for the practical adsorption of cationic dyes with its features of fast adsorption and high capacity.

* Corresponding author.
E-mail address: r-mukhlis@utm.my (M.A. Rahman).
Peer review under responsibility of King Saud University.

ELSEVIER Production and hosting by Elsevier

1. Introduction

Clean water is in high demand from industrial and domestic users. The effluents from the textile industry are exacerbating water pollution due to dyes, detergents, and other contaminants. The textile industry itself had consumed over 70,000

https://doi.org/10.1016/j.jscs.2020.09.006
1319-6103

tons of dyes to sustain textiles production [1,2]. The untreated dye wastewater undergoes chemical and biological changes, consumes dissolved oxygen, destroys aquatic life, and poses a threat to human health as many of these contaminants are highly toxic [3,4]. Thus, removing dyes from the wastewater before releasing to water stream is essential. Numerous methods are available for removing the dye from contaminated water, for example, chemical oxidation, flocculation, filtration, adsorption, and photodegradation [5]. Among them, adsorption is the most favourable method with a single-step operation, simple design, environmentally friendly, and economically feasible [6]. However, the interaction between adsorbent and dyes influences the efficiency of the adsorption process.

To date, the metal–organic framework (MOF), a relatively new class of porous material, had received substantial interest as an adsorbent in the adsorption field [7–9]. MOF is constructed by metal ions or metal clusters linked by organic ligand [10]. Their pore size, shape, dimensionality, and chemical environment can be finely controlled via a judicious selection of their building blocks (i.e., metal and organic linker). Then, the features of uniform porous structure with tunable pore size and large surface area had made it an emerging adsorbent compared to porous metal oxides [11]. Studies on dye adsorption of various MOFs have attempted to address the shortcomings of low stability inside the water. In present, a water-stable type MOF, MIL-101 (MIL: Material of Institute Lavoisier) can be constructed using different metal precursor, such as chromium (Cr) (MIL-101-Cr), aluminium (Al) (MIL-101-Al), and iron (Fe) (MIL-101-Fe). [16,17]. The hydrophilic properties of MIL-101 and the availability of Fe source at low cost with low toxicity had made MIL-101-Fe as a good candidate for this study [18].

Moreover, few strategies have been introduced to enhance the adsorption capability of the MOF. Such that by the functionalization of MOF with an active functional group. This can be simply done by introducing the functional group from the organic ligands. The different organic ligands used in synthesizing MOF, particularly for ligands containing functional group may interfere the physical properties in term of structural, BET surface, pores size, and even the adsorption properties of the synthesized MOF [11–13]. Previous comparative studies had investigated the adsorption activity between the non-functionalized and functionalized MOFs for dye removal. The studies report the active functional group of the functionalized MOF had played a crucial role in the increment of adsorption capacity [14,15].

At present, the comparative adsorption behaviour of pristine and functionalized MOF on dyes removal is less explored. In this work, the iron-based MIL-101 was synthesized. Then, the functionalization effect with an active group (amine group) is evaluated. Then, their potential towards the adsorption of methylene blue (MB) was investigated using adsorption isotherm, adsorption kinetic and recyclability.

2. Experimental

2.1. Materials

Iron chloride ($FeCl_3{\cdot}6H_2O$) purchased from Sigma Aldrich was used as a source of the iron precursor. Benzene dicarboxylic acid (H_2BDC) and 2-amino benzene dicarboxylic acid (NH_2-H_2BDC) purchased from ACROS ORGANICS were used as organic ligands. *N*,*N*-Dimethyl formamide (DMF) purchased from Sigma Aldrich was used as a solvent. Methylene blue was purchased from QRec. All the reagents were used without further purifications.

2.2. Synthesis of metal–organic frameworks

The iron-based metal–organic framework was prepared using the solvothermal method as described by a previous study with minor modification [19]. For synthesizing of non-functionalized MOF labelled as MOF-Fe, 2.45 mmol of $FeCl_3{\cdot}6H_2O$ and 1.24 mmol of BDC were dissolved in 30 mL of DMF. Then, the solution was transferred into a 250 mL Teflon bottle and placed in an oven for the solvothermal process at 120 °C for 24 h. The solvothermal solution was then cooled down to room temperature. The dull orange solid powder was collected by centrifugation and purified with DMF and ethanol and dried at 60 °C for 24 h. Meanwhile, for the functionalization of MOF-Fe with the amine group, the labelled amine-MOF-Fe was synthesized using the different organic linker of NH_2-H_2BDC with the same procedure explained for MOF-Fe.

2.3. Characterization

The physicochemical properties of MOF-Fe and amine-MOF-Fe were characterized using field emission scanning electron microscope (FESEM, JOEL JSM-6500F), X-ray diffraction (XRD, MiniFlex, Rigaku), Fourier-transform infrared spectroscopy (FTIR, Thermoscientific Nicolet 4700), and nitrogen adsorption–desorption (BET, BELSORP) analyses. Zeta potential (Malvern) analysis was conducted to obtain the isoelectronic point for both MOF-Fe and amine-MOF-Fe.

2.4. Adsorption of methylene blue

Stock solution (1000 mg/L) of methylene blue (MB) was prepared by dissolving in distilled water. The desired solution concentrations for further adsorption process were obtained by diluting the stock solution. The effect of various factors on MB adsorption such as the pH value of MB solution, contact time, MOFs loading, initial concentration, and the recyclability of the MOFs was studied. The adsorption process was conducted in the dark to avoid any possible photodegradation. After the adsorption, the dye-loaded adsorbent was separated using centrifugation at 7000 rpm for 5 min and 3 mL of the solution was taken for UV–visible spectrometer (JASCO V-650) measurement at 664 nm. The percentage (%) of MB adsorption and equilibrium adsorption capacity q_e (mg/g) was calculated according to Eq. (1) and Eq. (2), respectively [20]. Then, the adsorption kinetics and isotherm models were used to evaluate the experimental data. A possible mechanism of MB adsorption was also proposed.

$$\%Dye\ removal = \frac{C_0 - C_f}{C_0} \times 100 \tag{1}$$

$$q_e = \frac{(C_0 - C_e) \times V}{M} \tag{2}$$

where, C_0 is the initial feed concentration of dye solution, C_f is the final concentration of dye solution after adsorption, and C_e is the equilibrium concentration of dye solution (mg/L). Meanwhile, V is the volume of MB solution (L) and M is the mass of adsorbents (g).

2.5. Desorption of MB from loaded MOFs

The feasibility for regenerating the exhausted MOF-Fe and amine-MOF-Fe with MB was evaluated using solvent desorption technique. Pure ethanol was used as eluent to regenerate the MOFs particles [21]. After the first cycle of the adsorption process, the recovered MOFs particles were collected and dispersed in pure ethanol. Then, it was sonicated for 5 min, followed by a mild stirring for 1 h to complete the desorption process. Then, the MOFs particles were centrifuged at 7000 rpm for 5 min and dried at 100 °C for 2 h in a vacuum oven before being used for the next cycle of the adsorption process.

3. Results and discussion

3.1. Structural and properties of MOFs

The structure and particle size of the synthesized MOF-Fe and amine-MOF-Fe observed using FESEM are shown in Fig. 1. It can be clearly seen in Fig. 1(a, b) that MOF-Fe has a hexagonal spindle-like structure with an average length of 0.9–1.0 μm and a diameter of 0.5 μm. It is consistent with previous reports [19,22]. A slight structural change was observed for functionalized amine-MOF-Fe, with increased length of 1.897 μm and diameter of 0.451 μm but still maintaining the hexagonal spindle-like structure as shown in Fig. 1(c, d). The length elongation after amine functionalization was due to the different organic linkers with higher molecular weights; H_2BDC (166.13 g/mol) and NH_2-H_2BDC (181.15 g/mol).

Fig. 2(a) shows the XRD diffractogram of both MOF-Fe and amine-MOF-Fe. The main diffraction peaks displayed are in accordance with the data reported in the literature [23]. The similar exhibit diffraction patterns also indicate that the crystal phase structure was retained after amine functionalization. Besides, the XRD patterns suggest a better crystallinity for amino-functionalized amine-MOF-Fe compared to MOF-Fe as shown by the higher relative intensity of the peaks in the 6°–10° range. N_2 adsorption–desorption analysis is shown in Fig. 2(b). For MOF-Fe, the adsorption isotherm generated resembles to type I isotherm which clearly indicates microporous structure with a BET surface area of 447.59 m^2/g, the pore volume of 0.3652 cm^3/g, and pore size of 3.2641 nm. However, amine-MOF-Fe showed a type IV isotherm with mesoporous structure with a BET surface area of 16.329 m^2/g, the pore volume of 0.0729 cm^3/g, and pore size of 18.63 nm. The decrease in BET surface area for amine-MOF-Fe was due to the intrusion of $–NH_2$, as reported previously [24]. Besides, the bigger particles size of amine-MOF-Fe as observed in FESEM images also contributed to the decreased surface area. The BET data are listed in Table 1.

FTIR analysis was carried out to confirm the formation and bonding of amine on MOF-Fe and the FTIR spectra are shown in Fig. 3. Both MOF-Fe and amine-MOF-Fe consisted of benzenecarboxylates as they were synthesized using H_2BDC and NH_2-H_2BDC as organic ligands. Thus, both spectra observed reflect benzene-carboxylates (terephthalate ligands). The strong bands at 1598.70 and 1579.41 cm^{-1} for MOF-Fe and amine-MOF-Fe, respectively, indicate the C=O bonding in carboxylates [19]. While the bands at 1390.42 cm^{-1} for MOF-Fe and 1384.64 cm^{-1} for amine-

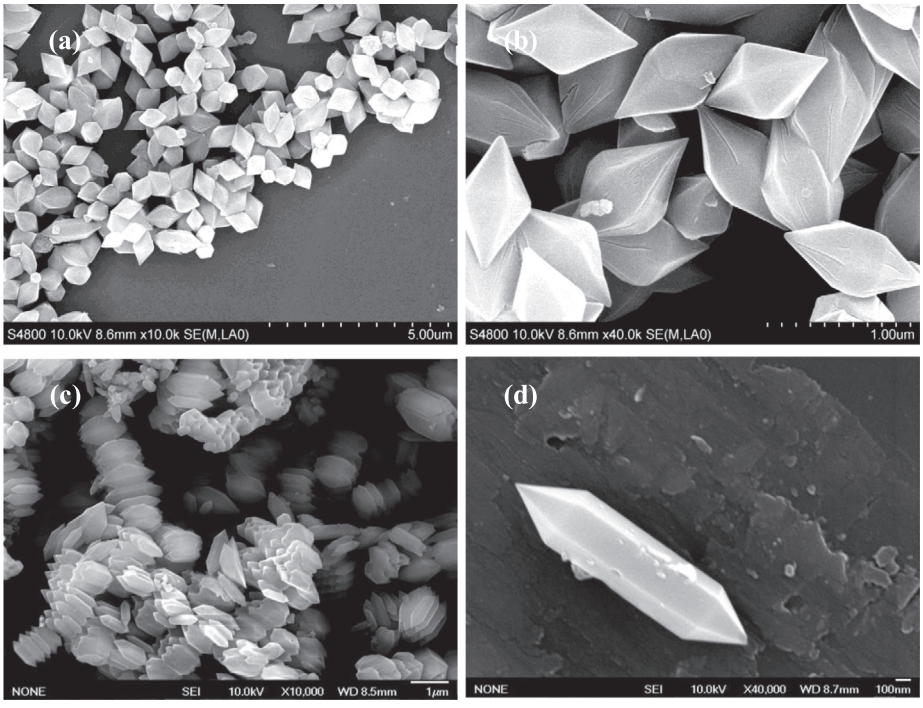

Fig. 1 FESEM images of (a, b) MOF-Fe and (c, d) amine-MOF-Fe.

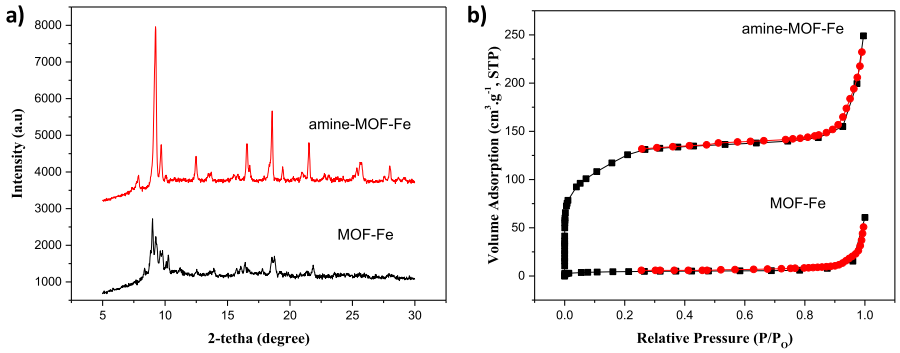

Fig. 2 (a) XRD diffractogram and (b) N_2 adsorption–desorption for MOF-Fe and amine-MOF-Fe.

Table 1 BET data analysis.

Sample	Surface area, S_{BET} (m^2/g)[a]	Pore volume, $V_{p.\ Total}$ (cm^3/g)[b]	Mean pore diameter, D_p (nm)[c]
MOF-Fe	447.59	0.3652	3.2641
Amine-MOF-Fe	16.329	0.0729	18.63

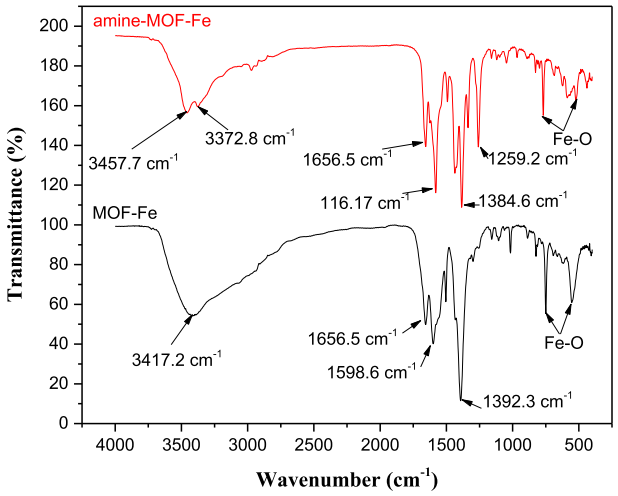

Fig. 3 FTIR spectra of MOF-Fe and amine-MOF-Fe.

MOF-Fe are associated with the vibrational mode of C–C [19]. As the benzene ring in amine-MOF-Fe was substituted with a primary amine, the spectrum also exhibited a band at approximately 1259.29 cm^{-1} which is assigned to the C–N stretching mode of aromatic amine. In addition, bands at 1621 and 1621.62 cm^{-1} for MOF-Fe and amine-MOF-Fe, respectively, are attributed to the N–H scissoring vibrations [25]. The broad absorption band at 3426.89 cm^{-1} for MOF-Fe corresponds to the hydroxyl moieties. While for amine-MOF-Fe, the presence of amino groups in their free unassociated form is indicated by the bands located at 3457.74 and 3446.17 cm^{-1} which correspond to the asymmetric and symmetric N–H stretching modes, respectively. The apparent peaks at 540–750 cm^{-1} are related to the Fe–OH vibration [23]. These FTIR spectra are in a good agreement with the data reported in a report confirming the formation of Fe-based MOFs with and without amine functionalization [26].

3.2. Adsorption of MB solution

3.2.1. Effects of pH

The pH-dependent MB uptake is an important parameter for dye adsorption study. A series of adsorption test was conducted on the MB solution in the pH range of 3–10. The initial concentration and MOFs loading were set constant at 20 mg/L and 0.2 g/L, respectively. The results are shown in Fig. 4(a) showed the increases of adsorption capacities for both MOF-Fe and amine-MOF-Fe at increasing pH value of MB solution. Such behaviour is attributed by the electrostatic interactions between the charged surfaces of MOFs and MB. The isoelectronic points (IEP) of MOF-Fe and amine-MOF-Fe indicate that the pH value at the point of zero charges (pH_{pzc}) were 7.1 and 7.4, respectively as shown in Fig. 4(b). Herein, at a pH of lower than the pH_{pzc} of adsorbent ($pH < pH_{pzc}$), the adsorbent surface will be positively charged because of the hydrogen ions (H^+) adsorption or the reaction of H^+ ions with the surface functional group (hydroxyl groups). It is vice versa at a pH solution higher than the pH_{pzc} of adsorbent ($pH > pH_{pzc}$), where deprotonating on the adsorbent surface occurs. In this case, a higher pH of MB solution is favourable for MB removal because at high pH, the number of negatively charged sites increases which favours the positively charged MB ions due to the electrostatic force of attraction. The higher adsorption capacity of amine-MOF-Fe was due to a more negative zeta potential value compared to that of MOF-Fe [14].

3.2.2. Effect of contact time and adsorption kinetic

The time factor on MB adsorption was evaluated at pH 9 of MB solution, MB initial concentration of 20 mg/L, and MOFs loading of 0.2 g/L. A rapid increase of adsorption capacity was measured at 30 and 75 mg/g for both MOF-Fe and amine-MOF-Fe within the first hour of the adsorption process, respectively as shown in Fig. 5. As the contact time was prolonged to 24 h, the adsorption became slower until equilibrium at 15 h and 10 h with the adsorption capacities of 56.23 and 98.87 mg/g for MOF-Fe and amine-MOF-Fe, respectively. It is evident that the adsorption process involved several stages. Sorption process started with a fast dye removal due to the

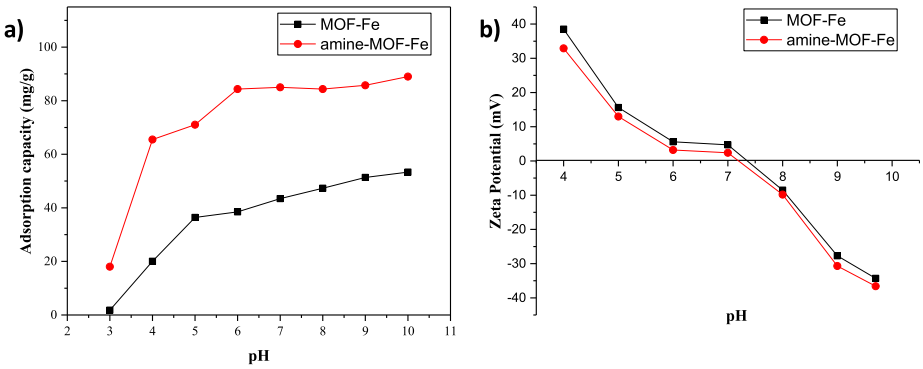

Fig. 4 (a) Adsorption capacities for MB removal at different pH values and (b) zeta potentials of MOF-Fe and amine-MOF-Fe.

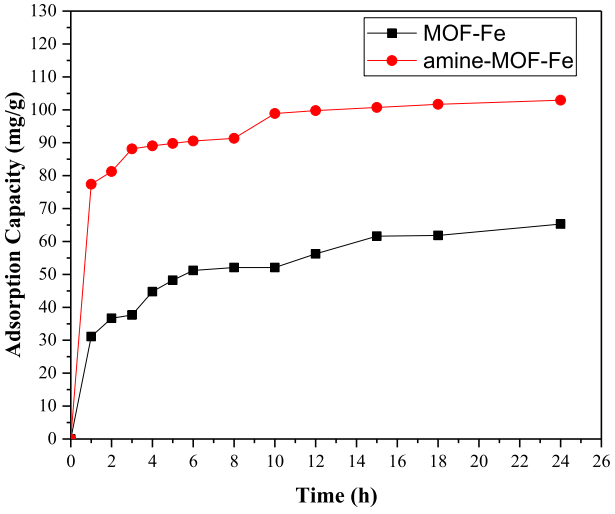

Fig. 5 Adsorption capacities of MOF-Fe and amine-MOF-Fe.

availability of numerous unoccupied active sites on the adsorbent [21]. The adsorption capacities obtained in the first stage were higher than those reported earlier, obviously reflecting the advantages of the synthesized MOF-Fe and amine-MOF-Fe in this study.

The kinetics data obtained were analyzed to understand the adsorption behaviour using pseudo-first-order kinetics, pseudo-second-order kinetics, and intraparticle diffusion by Weber and Morris model using the simplified Eq. (3), Eq. (4) and Eq. (5), respectively [27].

$$ln(q_e - q_t) = lnq_e - k_1 t \tag{3}$$

$$\frac{t}{q_t} = \frac{1}{k_2 q_e^2} + \frac{1}{q_e} t \tag{4}$$

$$q_t = k_{id}\sqrt{t} + I \tag{5}$$

where, q_e is the adsorption capacity at equilibrium, q_t is the adsorption capacity at time t, t is the contact time, k_1 is the first-order equilibrium constant, k_2 is the second-order equilibrium constant, k_{id} is intraparticle diffusion rate constant (mg/g•min$^{-1/2}$), and I is the slope that represents the thickness of the boundary layer.

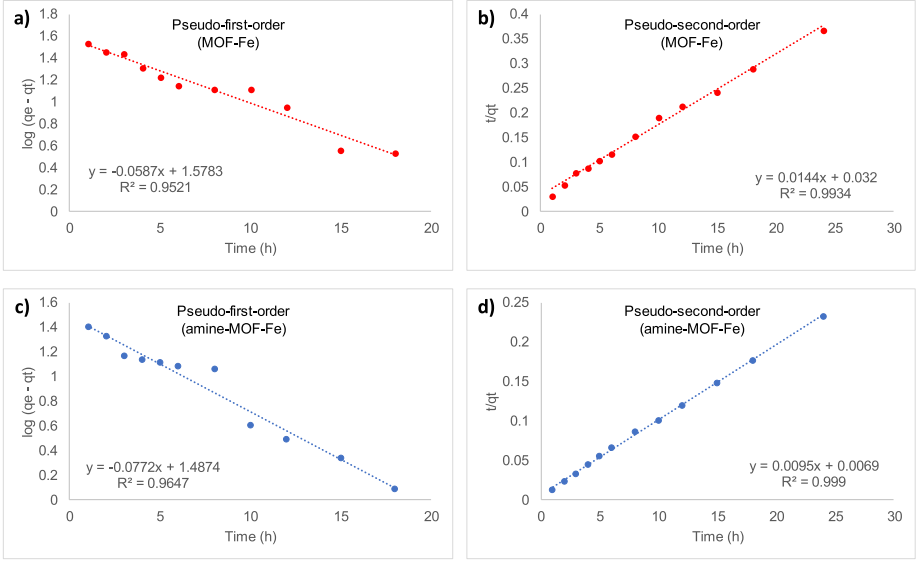

Fig. 6 The pseudo-first-order (a, c) and pseudo-second-order (b, d) plot of MB adsorption for (●) MOF-Fe and (●) amine-MOF-Fe.

Table 2 Pseudo-first- and pseudo-second-order kinetic parameters for MB adsorption using MOF-Fe and amine-MOF-Fe.

MOF	Pseudo-first-order				Pseudo-second-order			
	$q_{e,exp}$ (mg/g)	k_1	$q_{e,cal}$ (mg/g)	R^2	$q_{e,exp}$ (mg/g)	k_2	$q_{e,cal}$ (mg/g)	R^2
MOF-Fe	65.311	0.135	37.870	0.9521	65.311	0.006481	69.4444	0.9934
Amine-MOF-Fe	102.925	0.1778	30.718	0.9647	102.925	0.013080	105.2632	0.9990

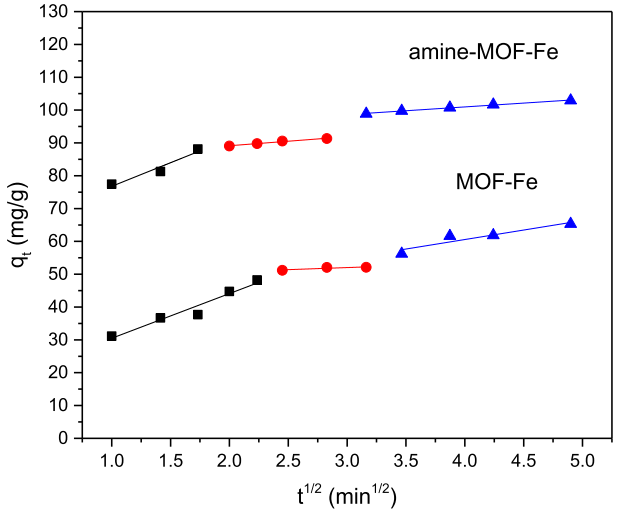

Fig. 7 Weber and Morris intraparticle diffusion plot for the adsorption of MB using both MOF-Fe and amine-MOF-Fe.

The constant values (k) obtained from the plot of $\log(q_e - q_t)$ versus t for the pseudo-first-order model in Fig. 6(a, c) and the plot of t/q_t versus t for the pseudo-second-order model in Fig. 6(b, d) and the other parameters for both kinetic isotherms are listed in Table 2. For both MOFs (MOF-Fe and amine-MOF-Fe), the pseudo-second-order best fitted with a preferable coefficient R^2 value of 0.9934 and 0.9990, respectively. In addition, the calculated value for equilibrium adsorption capacity (q_e) and the experimental q_e values are almost similar for both MOFs, confirming the satisfactory of the pseudo-second-order model. The results of the adsorption kinetics provide a view on the adsorption mechanisms. The pseudo-second-order kinetic model is based on the amount of dye adsorbed on the surface of the adsorbent and the adsorption capacity at the equilibrium. Further, the k_2 value of amine-MOF-Fe is two times higher than that of MOF-Fe which indicates the affinity of MOF-Fe towards MB is weaker compared to amine-MOF-Fe. This is similar to the reported NH_2-UiO-66 [14].

The plot of q_t versus $t^{1/2}$ for intraparticle diffusion proposed by Weber and Morris [11] is shown in Fig. 7. According to this model, if the linear straight line passes through the origin, the intraparticle diffusion is controlling the entire adsorption process. However, in the present data, the lines have nonzero intercepts which indicate the adsorption process may involve more than one mechanism. The first straight line represents the initial surface adsorption. Then, the second straight line represents the intraparticle diffusion. Lastly, the third line corresponds to the final equilibrium stage of adsorption.

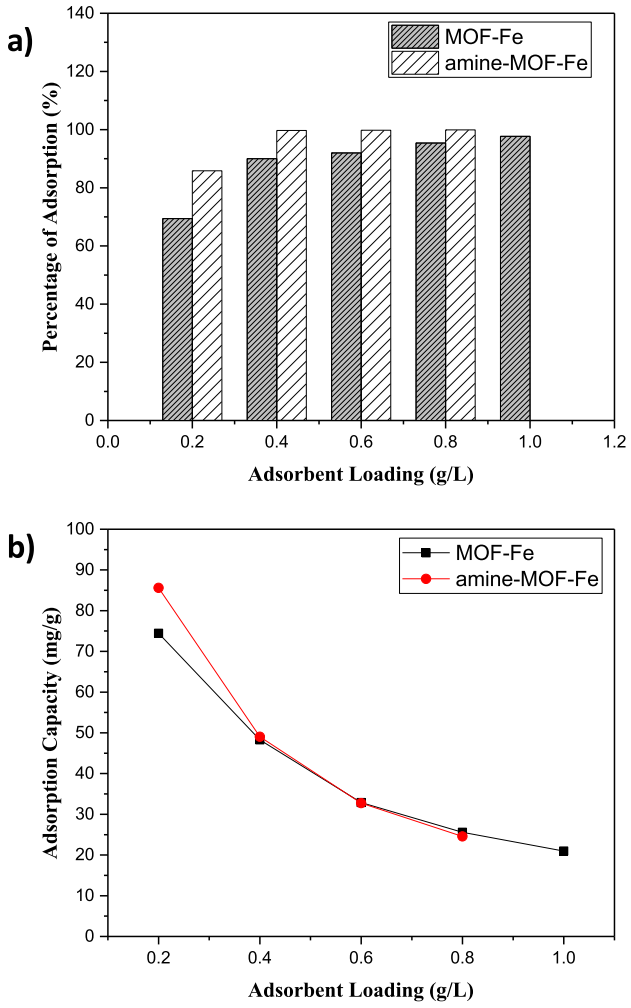

Fig. 8 (a) MB removal and (b) adsorption capacity at different MOFs loadings.

3.2.3. *Effect of adsorbent loading*

Fig. 8 shows the percentage of MB removal and the adsorption capacity as a function of MOFs loading. Fig. 8(a) shows the increased MB removal as the amount of MOF-Fe loading was increased due to the increase of available adsorption sites. For amine-MOF-Fe, the same trend was observed but at the loading of 0.4–0.8 g/L, this amine-functionalized MOF-Fe yielded a constant ~99.9% of MB removal. Increasing the MOF loading, the adsorption capacity decreased (Fig. 8b). It is understood that the number of available adsorption sites increases by increasing the adsorbent loading, resulting in an increase of the MB removal. This is due to the adsorption sites

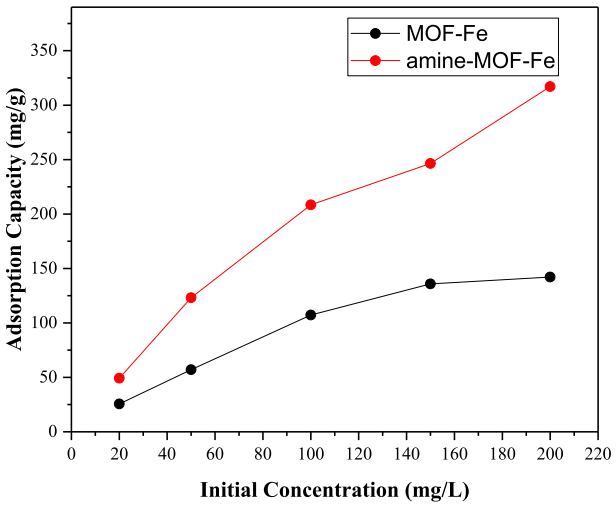

Fig. 9 Effect of different initial concentrations on the adsorption capacity of MB.

available remained unsaturated during the adsorption process. For MOF-Fe, the percentage of removal achieved its saturation point at 0.8 g/L. The results show that the amine-functionalized MOF gave better MB removal at adsorbent loading 2 times lower than that of the non-functionalized MOF, where, MOF-Fe and amine-MOF-Fe achieved their saturation points at 0.8 and 0.4 g/L of MOF loadings, respectively.

3.2.4. Effect of initial concentration and adsorption isotherm

Fig. 9 shows the plot of adsorption capacity versus the initial concentration of MB for MOF-Fe and amine-MOF-Fe. The increases of the adsorption capacity with the increases in the initial concentration of MB solution were observed. For MOF-Fe, the adsorption capacity was stable at the initial concentration of 150 mg/L which indicates the saturation of adsorption capacity at higher concentration. Moreover, the measured equilibrium adsorption capacity for amine-MOF-Fe was two times higher than that for MOF-Fe due to the introduction of $-NH_2$ which was available as additional adsorption sites for cationic MB.

Langmuir and Freundlich's isotherms were employed to model the adsorption of MB using Eq. (6) and Eq. (7), respectively.

$$\frac{C_e}{q_e} = \frac{C_e}{q_m} + \frac{1}{bq_m} \tag{6}$$

$$q_e = K_F C_e^{1/n} \tag{7}$$

where, C_e is the concentration at equilibrium (mg/L), q_e is the adsorption capacity at equilibrium (mg/g), q_m is the adsorption at maximum (mg/L), b is the constant value for Langmuir, and K_F is the constant for Freundlich. Meanwhile, to determine whether the adsorption process is favourable or unfavourable, the separation factor parameter, R_L was calculated using Eq. (8).

$$R_L = \frac{1}{1 + K_L C_0} \tag{8}$$

where, K_L is the Langmuir constant and C_0 is the initial MB concentration (mg/L). The plot C_e/q_e versus C_e for Langmuir isotherm and the plot ln q_e versus C_e for Freundlich isotherm are presented in Fig. 10. The parameters for both adsorption isotherms are listed in Table 3. Langmuir isotherm assumes that adsorption process is monolayer and occurs on a homogeneous surface with all the adsorption sites possessing identical affinities for the adsorbate [28,29]. Freundlich isotherm model explains the adsorption process occurs on the heterogeneous surface with multilayer adsorption [30]. For MOF-Fe, the adsorption followed Langmuir isotherm with the highest correlation coefficient (R^2 = 0.9994). The R_L value indicates the adsorption to be unfavorable when $R_L > 1$, linear when $R_L = 1$, favorable when $0 < R_L < 1$, and irreversible when $R_L = 0$ [11,31]. Meanwhile, for amine-MOF-Fe, the adsorption followed Freundlich isotherm with the highest correlation coefficient (R^2 = 0.9935). The larger the n value, the more feasible the adsorption is.

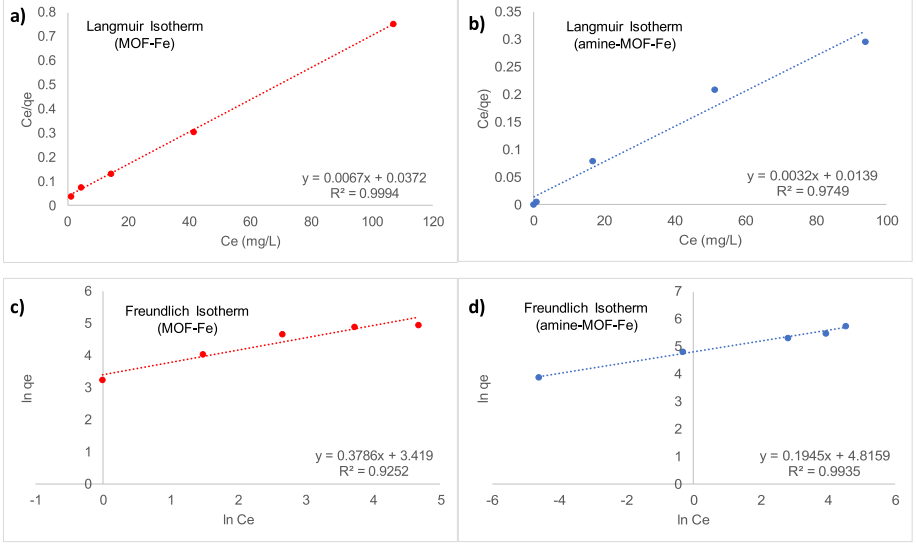

Fig. 10 (a and b) Langmuir and (c and) Freundlich adsorption isotherms of MB for MOF-Fe (●) and amine-MOF-Fe (●).

Table 3 Langmuir and Freundlich adsorption isotherms parameters for MB adsorption using MOF-Fe and amine-MOF-Fe.

MOF	Langmuir				Freundlich		
	q_{max} (mg/g)	b	R^2	R_L	N	k_F	R^2
MOF-Fe	149.25	0.1801	0.9994	0.0359	2.6413	30.5389	0.9252
Amine-MOF-Fe	312.5	0.2302	0.9749	0.0137	5.1414	123.4579	0.9935

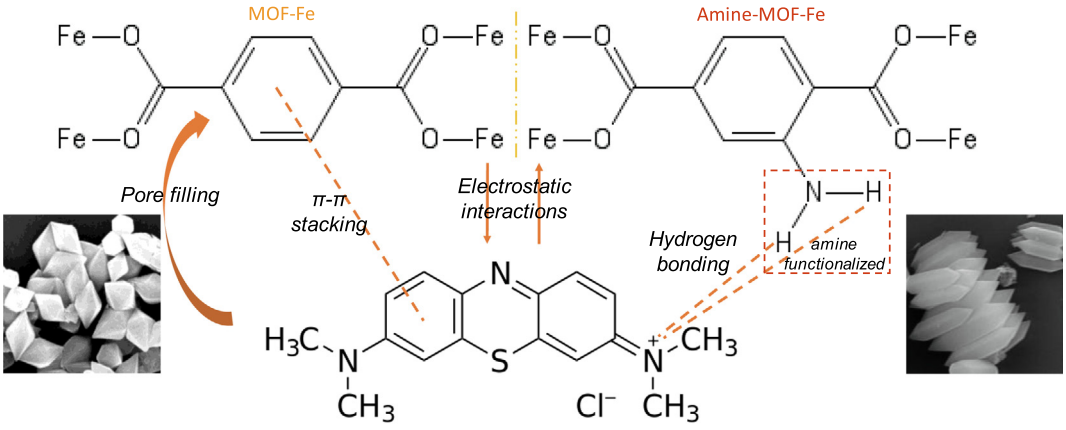

Fig. 11 Possible mechanisms of MB adsorption on MOF-Fe and amine-MOF-Fe.

3.2.5. Mechanism of MB adsorption

The organically porous structure of MOFs drives the adsorption process by pore-filling mechanism [32]. However, in this work, several probable mechanisms were proposed to understand the mechanism of solid MOF and MB molecules in aqueous solution. Based on the effect of pH solution, contact time, initial concentration of MB solution, and the evaluation of the adsorption kinetics and isotherms for both MOFs, the proposed mechanisms of MB adsorption on MOF-Fe and amine-MOF-Fe are illustrated in Fig. 11. The electrostatic interaction was seen as the main adsorption factor confirmed by the increases in the adsorption capacity as the pH value of the MB solution was increased. MB can migrate from the aqueous solution through the pore channels of MOFs to reach almost all of the potential adsorptive sites. The higher adsorption capacity of amine-MOF-Fe than that of MOF-Fe was not only due to the electrostatic interaction and pore-filling interaction, but also the hydrogen bonding interaction [33]. Also, the electrostatic interaction with the electron lone pairs on the $-NH_2$ groups of the functionalized MOF had played a role to increase the adsorption capacity. This may be due the $-NH_2$ group on the framework of amine-MOF-Fe that is ready to accept hydrogen proton and form positively charged $-NH^{3+}$, facilitating the interaction with MB through electrostatic attraction. Lastly, the π–π staking interactions between aromatic rings of MB and MOFs also existed to facilitate the adsorption process [34]. Hence, it can be concluded that different interactions such as pore filling, electrostatic interaction, hydrogen bonding, and π–π stacking were responsible to facilitate the adsorption of MB on MIL-101-Fe and NH_2-MIL-101-Fe. The comparative study of different MOFs with the present study for MB removal is listed in Table 4.

3.2.6. Recyclability of MOFs on MB adsorption

The reusability of an adsorbent is another important criterion in the adsorption process. Thus, the adsorption/desorption process for MOF-Fe and amine-MOF-Fe was carried out using 10 mg/L of MB solution at pH 9. After 6 h of the adsorption process, both MOFs were recovered using centrifugation. Then, the desorption process was carried out. Fig. 12 shows the adsorption percentage of MB for both MOF-Fe and amine-MOF-Fe after being used for three times. The regeneration results obtained for MOF-Fe show an increase in the MB removal after being repeatedly washed and used for the next cycles. This phenomenon is rarely reported but this may be due to the high surface area of MOF-Fe compared to amine-MOF-Fe which required repeated washing and drying under vacuum to completely remove the guest molecules inside the porous structure of MOF-Fe [36]. However, the regeneration

Table 4 MB adsorption using different MOFs.

Type of MOFs	Adsorption and kinetics isotherm	Adsorption capacity (mg/g)	Ref.
Cu-BTC	Freundlich/pseudo-second-order	96.4	[8]
UiO-66	Langmuir/pseudo-second-order	107	[35]
HKUST-1	Langmuir/pseudo-second-order	454	
MOF-Fe Amine-MOF-Fe	Langmuir Freundlich	149.25 312.5	This study

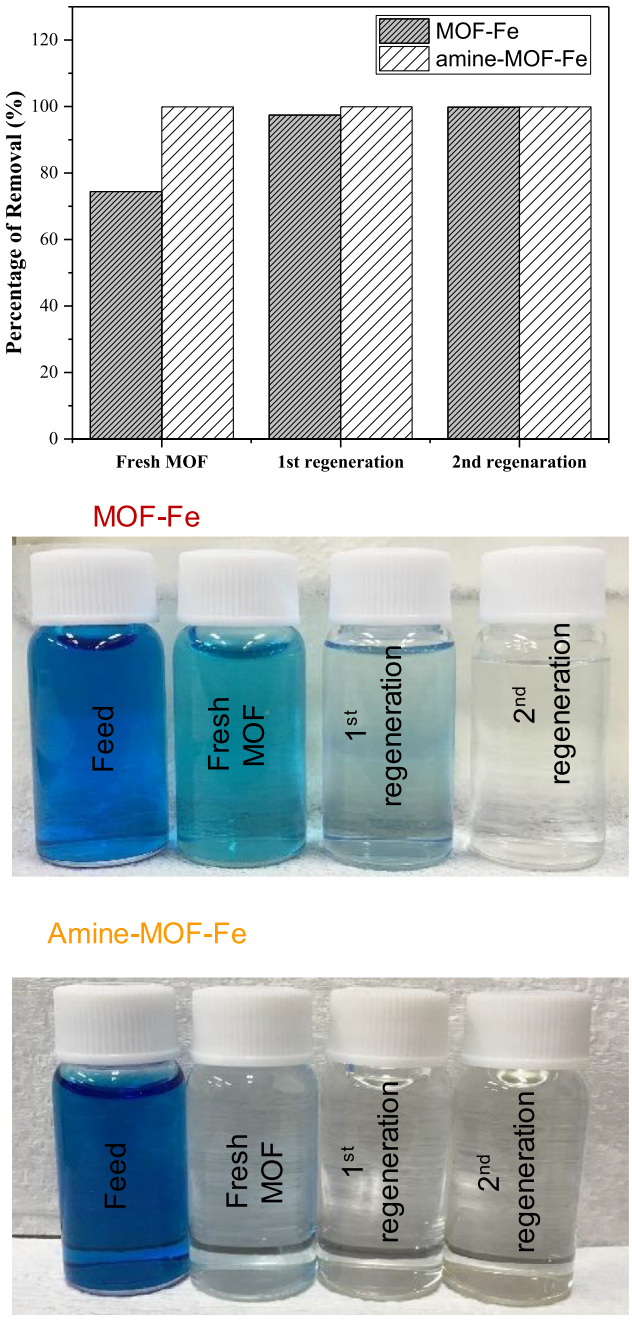

Fig. 12 The regeneration of MB solution using for both MOF-Fe and amine-MOF-Fe.

results for the adsorption by amine-MOF-Fe remained the same after being regenerated and used for two times. Hence, the results indicate that both MOFs had desirable reusability for the practical adsorption of cationic dyes.

4. Conclusion

Hazardous dye (MB) can be efficiently removed from the contaminated water via adsorption process. The synthesized MOF-Fe and amine-MOF-Fe synthesized in this study had shown a high adsorption capacity for cationic MB of 149.25 and 312.5 mg/g, respectively. The effect of amine-functionalization had proved that the amine group played an indispensable role in the adsorption process as yielded two times higher adsorption capability towards MB ions. Moreover, the MOF loading can be reduced into the half when the MOF-Fe is functionalized with the amine group. The adsorption isotherm revealed that the Langmuir isotherm had best described for MOF-Fe. Meanwhile, the Freundlich isotherm had best described for amine-MOF-Fe. Besides, the adsorption kinetic had shown both MOFs followed the pseudo-second-order kinetics model. Attempts to reuse both MOFs had demonstrated that amine-MOF-Fe could maintain adsorption performance after two-cycle. Nevertheless, both MOFs are a promising adsorbent for cationic dyes removal from the aqueous solution.

Declaration of Competing Interest

The authors declare that they have no known competing financial interests or personal relationships that could have appeared to influence the work reported in this paper.

Acknowledgements

The authors gratefully acknowledge the financial support from various parties, namely, the Islamic Educational, Scientific and Cultural Organization (ISESCO) (R.J130000.7351.4B368), Malaysia Ministry of Higher Education (MOHE) through Malaysian Research University Network (MRUN) grant (R.J130000.7851.4L864), the Higher Institution Centre of Excellence (HICoE) Research Grant (R.J090301.7851.4J422), and Universiti Teknologi Malaysia (UTM) through the Research University grant (Q.J130000.2446.04G30, Q.J130000.3551.05G77, Q.J130000.3051.01M47). Appreciation also goes to UTM Research Management Centre for both financial and technical supports.

References

[1] M.T. Yagub, T.K. Sen, S. Afroze, H.M. Ang, Dye and its removal from aqueous solution by adsorption: a review, Adv. Colloid Interface Sci. 209 (2014) 172–184, https://doi.org/10.1016/j.cis.2014.04.002.

[2] M. Rafatullah, O. Sulaiman, R. Hashim, A. Ahmad, Adsorption of methylene blue on low-cost adsorbents: a review, J. Hazard. Mater. 177 (2010) 70–80, https://doi.org/10.1016/j.jhazmat.2009.12.047.

[3] D. Jiang, M. Chen, H. Wang, G. Zeng, D. Huang, M. Cheng, Y. Liu, W. Xue, Z. Wang, The application of different typological and structural MOFs-based materials for the dyes adsorption, Coord. Chem. Rev. 380 (2019) 471–483, https://doi.org/10.1016/j.ccr.2018.11.002.

[4] A. Srinivasan, T. Viraraghavan, Decolorization of dye wastewaters by biosorbents: a review, J. Environ. Manage. 91 (2010) 1915–1929, https://doi.org/10.1016/j.jenvman.2010.05.003.

[5] V. Katheresan, J. Kansedo, S.Y. Lau, Efficiency of various recent wastewater dye removal methods: a review, J. Environ. Chem. Eng. 6 (2018) 4676–4697, https://doi.org/10.1016/j.jece.2018.06.060.

[6] H. Liu, L. Chen, J. Dang, Adsorption behavior of magnetic amino-functionalized metal-organic framework for cationic and

anionic dyes from aqueous solution, RSC Adv. (2016), https://doi.org/10.1039/C6RA07567C.
[7] H. Saleem, U. Rafique, R.P. Davies, Investigations on post-synthetically modified UiO-66-NH for the adsorptive removal of heavy metal ions from aqueous solution, Microporous Mesoporous Mater. 221 (2016) 238–244, https://doi.org/10.1016/j.micromeso.2015.09.043.
[8] R. Kaur, A. Kaur, A. Umar, W.A. Anderson, Metal organic framework (MOF) porous octahedral nanocrystals of Cu-BTC: Synthesis, properties and enhanced adsorption properties, Mater. Res. Bull. 109 (2019) 124–133, https://doi.org/10.1016/j.materresbull.2018.07.025.
[9] D. Chen, P. Fei Feng, F. Hua Wei, Preparation of Fe(III)-MOFs by microwave-assisted ball for efficiently removing organic dyes in aqueous solutions under natural light, Chem. Eng. Process. - Process Intensif. 135 (2019) 63–67. doi:10.1016/j.cep.2018.11.013.
[10] R.J. Kuppler, D.J. Timmons, Q. Fang, J. Li, T.A. Makal, M.D. Young, D. Yuan, D. Zhao, W. Zhuang, H. Zhou, Potential applications of metal-organic frameworks, Coord. Chem. Rev. 253 (2009) 3042–3066, https://doi.org/10.1016/j.ccr.2009.05.019.
[11] X. Luo, S. Fu, Y. Du, J. Guo, B. Li, Adsorption of methylene blue and malachite green from aqueous solution by sulfonic acid group modified MIL-101, Microporous Mesoporous Mater. 237 (2017) 268–274, https://doi.org/10.1016/j.micromeso.2016.09.032.
[12] B.D. Hong, Y.K. Hwang, C. Serre, J. Chang, Porous chromium terephthalate MIL-101 with coordinatively unsaturated sites: surface functionalization, encapsulation, sorption and catalysis, Adv. Funct. Mater. 19 (2009) 1537–1552, https://doi.org/10.1002/adfm.200801130.
[13] I. Ahmed, S.H. Jhung, Effective adsorptive removal of indole from model fuel using a metal-organic framework functionalized with amino groups, J. Hazard. Mater. 283 (2015) 544–550, https://doi.org/10.1016/j.jhazmat.2014.10.002.
[14] Q. Chen, Q. He, M. Lv, Y. Xu, H. Yang, X. Liu, F. Wei, Selective adsorption of cationic dyes by UiO-66-NH_2, Appl. Surf. Sci. 327 (2015) 77–85, https://doi.org/10.1016/j.apsusc.2014.11.103.
[15] E. Haque, V. Lo, A.I. Minett, A.T. Harris, T.L. Church, Dichotomous adsorption behaviour of dyes on an amino-functionalised metal-organic framework, amino-MIL-101(Al), J. Mater. Chem. A 2 (2014) 193–203, https://doi.org/10.1039/c3ta13589f.
[16] Z. Li, X. Liu, W. Jin, Q. Hu, Y. Zhao, Adsorption behavior of arsenicals on MIL-101(Fe): the role of arsenic chemical structures, J. Colloid Interface Sci. 554 (2019) 692–704, https://doi.org/10.1016/j.jcis.2019.07.046.
[17] T. Zhao, L. Yang, P. Feng, I. Gruber, C. Janiak, Y. Liu, Facile synthesis of nano-sized MIL-101(Cr) with the addition of acetic acid, Inorg. Chim. Acta 471 (2018) 440–445, https://doi.org/10.1016/j.ica.2017.11.030.
[18] P.A. Konik, E.A. Berdonosova, I.M. Savvotin, S.N. Klyamkin, The influence of amide solvents on gas sorption properties of metal-organic frameworks MIL-101 and ZIF-8, Microporous Mesoporous Mater. 277 (2019) 132–135, https://doi.org/10.1016/j.micromeso.2018.10.026.
[19] E. Rahmani, M. Rahmani, Alkylation of benzene over Fe-based metal organic frameworks (MOFs) at low temperature condition, Microporous Mesoporous Mater. 249 (2017) 118–127.
[20] F. Tan, M. Liu, K. Li, Y. Wang, J. Wang, X. Guo, G. Zhang, C. Song, Facile synthesis of size-controlled MIL-100 (Fe) with excellent adsorption capacity for methylene blue, Chem. Eng. J. 281 (2015) 360–367, https://doi.org/10.1016/j.cej.2015.06.044.
[21] E. Yılmaz, E. Sert, F.S. Atalay, Synthesis, characterization of a metal organic framework : MIL-53 (Fe) and adsorption mechanisms of methyl red onto MIL-53 (Fe), J. Taiwan Inst. Chem. Eng. 65 (2016) 323–330.
[22] Z. Zhang, X. Li, B. Liu, Q. Zhao, G. Chen, Hexagonal microspindle of NH_2-MIL-101(Fe) metal–organic frameworks with visible-light- induced photocatalytic activity for the degradation of toluene, RSC Adv. 6 (2016) 4289–4295, https://doi.org/10.1039/C5RA23154J.
[23] A.D.S. Barbosa, D. Julião, D.M. Fernandes, A.F. Peixoto, C. Freire, B. de Castro, C.M. Granadeiro, S.S. Balula, L. Cunha-Silva, Catalytic performance and electrochemical behaviour of Metal–organic frameworks: MIL-101(Fe) versus NH_2-MIL-101 (Fe), Polyhedron 127 (2017) 464–470, https://doi.org/10.1016/j.poly.2016.10.032.
[24] M. Almá, V. Zele, P. Palotai, E. Be, A. Zele, Metal-organic framework MIL-101 (Fe) -NH 2 functionalized with different long-chain polyamines as drug delivery system, Inorg. Chem. Commun. 93 (2018) 115–120, https://doi.org/10.1016/j.inoche.2018.05.007.
[25] R. Liu, L. Chi, X. Wang, Y. Wang, Y. Sui, T. Xie, H. Arandiyan, Effective and selective adsorption of phosphate from aqueous solution via trivalent-metals-based amino-MIL-101 MOFs, Chem. Eng. J. 357 (2019) 159–168, https://doi.org/10.1016/j.cej.2018.09.122.
[26] P. Karthik, A. Pandikumar, M. Preeyanghaa, M. Kowsalya, B. Neppolian, Amino-functionalized MIL-101(Fe) metal-organic framework as a viable fluorescent probe for nitroaromatic compounds, Microchim. Acta 184 (2017) 2265–2273, https://doi.org/10.1007/s00604-017-2215-2.
[27] A.A. Jalil, S. Triwahyono, S.H. Adam, N.D. Rahim, M.A.A. Aziz, N.H.H. Hairom, N.A.M. Razali, M.A.Z. Abidin, M.K.A. Mohamadiah, Adsorption of methyl orange from aqueous solution onto calcined Lapindo volcanic mud, J. Hazard. Mater. 181 (2010) 755–762, https://doi.org/10.1016/j.jhazmat.2010.05.078.
[28] R.M. Ali, H.A. Hamad, M.M. Hussein, G.F. Malash, Potential of using green adsorbent of heavy metal removal from aqueous solutions: adsorption kinetics, isotherm, thermodynamic, mechanism and economic analysis, Ecol. Eng. 91 (2016) 317–332, https://doi.org/10.1016/j.ecoleng.2016.03.015.
[29] Z. Yang, L. Zhu, L. Chen, Selective adsorption and separation of dyes from aqueous solution by core-shell structured NH_2-functionalized UiO-66 magnetic composites, J. Colloid Interface Sci. 539 (2019) 76–86, https://doi.org/10.1016/j.jcis.2018.11.064.
[30] Y. Liu, Y. Kang, B. Mu, A. Wang, Attapulgite / bentonite interactions for methylene blue adsorption characteristics from aqueous solution, Chem. Eng. J. 237 (2014) 403–410, https://doi.org/10.1016/j.cej.2013.10.048.
[31] A. Kumar, U. Kumar, K. Kumar, D. Banerjee, Removal of textile dyes by carbon nanotubes: a comparison between adsorption and UV assisted photocatalysis, Phys. E Low-Dimensional Syst. Nanostruct. 99 (2018) 6–15, https://doi.org/10.1016/j.physe.2018.01.008.
[32] J.G. and E. Besley, Pore-filling contamination in metal-organic frameworks, Phys. Chem. Chem. Phys. 20 (2018) 23616–23624. doi:10.1039/b000000x/.
[33] Q. Gao, J. Xu, X.H. Bu, Recent advances about metal–organic frameworks in the removal of pollutants from wastewater, Coord. Chem. Rev. 378 (2018) 17–31, https://doi.org/10.1016/j.ccr.2018.03.015.
[34] K.A. Lin, H. Chang, C. Hsu, Iron-based metal organic framework, MIL-88A, as a heterogeneous persulfate catalyst for decolorization of Rhodamine B in water, RSC Adv. 5 (2015) 32520–32530, https://doi.org/10.1039/c5ra01447f.
[35] M. Rizwan, H. Rasool, H. Sun, V. Periasamy, M.O. Tadé, S. Wang, One-pot synthesis of binary metal organic frameworks (HKUST-1 and UiO-66) for enhanced adsorptive removal of water contaminants, J. Colloid Interface Sci. 490 (2017) 685–694.
[36] P. Kumar, B. Anand, Y.F. Tsang, K.H. Kim, S. Khullar, B. Wang, Regeneration, degradation, and toxicity effect of MOFs: opportunities and challenges, Environ. Res. 176 (2019), https://doi.org/10.1016/j.envres.2019.05.019 108488.